Supplement of Atmos. Chem. Phys., 21, 6999–7022, 2021
https://doi.org/10.5194/acp-21-6999-2021-supplement

Atmospheric Chemistry and Physics
Open Access

Supplement of

Water uptake of subpollen aerosol particles: hygroscopic growth, cloud condensation nuclei activation, and liquid–liquid phase separation

Eugene F. Mikhailov et al.

Correspondence to: Eugene F. Mikhailov (eugene.mikhailov@spbu.ru)

Supplementary material

S1 Surface material of pollen grains

Pollen grains contain gluing material on their surface. Gluing material, also called polencoat, derives from secretion and degeneration of the anther tapetum, and includes pollenkitt, tryphine and elastovoscin (Pacini, E., and Franchi, 1993). Pollenkitt is formed when tapetal cell plasmamembranes rupture after complete degeneration of tapetal protoplasts (Piffanelli et al., 1998). It is the most common pollen glue for angiosperm plants, like rapeseed and birch used in this study (Fig. S1).

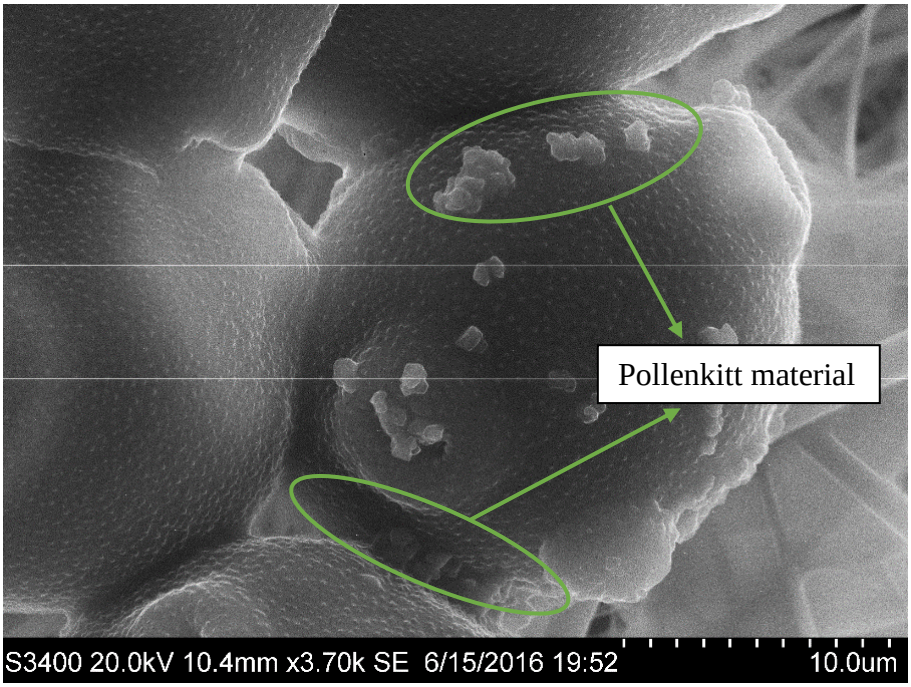

Fig. S1 SEM image of birch pollen grains. Pollenkitt compounds form a glue bridge between grains.

Pollenkitt consist of a number of organic compounds including saturated and unsaturated lipids, carotenoids, flavonoids, proteins and sugars (Chichiriccò et al., 2019). The tapetal cytoplasm may disappear without giving rise to any fatty substance and is therefore reabsorbed by the pollen grains surface. Elaioplats, spherosomes and other cell components are mainly present on the surface of the gymnosperm grains, such as pine pollen (Pacini and Hesse, 2005).

S2 Penetrated and captured pollen mass upon filtration

The mass of penetrated pollen species (total solid, TS) was determined as the difference between the initial pollen mass and the mass captured by the syringe filter. The average MR and standard deviation (SD) is the result of three measurements for each sample.

Table S1. Filtration protocol of the pollen aqueous solution. Three series of measurements performed for each type of pollen. *MR* is the ratio of the penetrated mass to the initial mass of pollen.

Pollen type	Initial pollen mass at 30 % RH	Blank filter mass at 30 % RH	Filter mass loading after 24h vacuum drying and exposure at 30 % RH	Filter captured pollen mass	Penetrated pollen mass	*MR*	
	mg	mg	mg	mg	mg		
	99.92	2548.01	2615.57	67.56	32.36		0.324
	100.09	2501.81	2569.22	67.37	32.72		0.324
Birch	100.16	2539.74	2607.22	67.48	32.68		0.326
						Average	**0.326**
						SD	**0.002**
	100.16	2505.80	2576.42	70.62	29.54		0.295
	100.06	2509.45	2579.97	70.52	29.54		0.295
Pine	100.17	2530.75	2602.77	72.02	28.15		0.282
						Average	**0.290**
						SD	**0.008**
	100.08	2498.13	2551.80	53.67	46.41		0.464
	100.05	2523.11	2576.15	53.04	47.01		0.470
Rapeseed	100.06	2507.88	2561.79	53.91	46.15		0.461
						Average	**0.465**
						SD	**0.004**

S3. HHTDMA setup and modes of operation

Figure S2 shows a sketch of the HHTDMA setup. Both DMAs thermally insulated and operated with a closed loop sheath air setup. The sheath and aerosol flow rates in both DMAs were 3.0 and 0.3 l min^{-1}, respectively. To control the RH we used a dew point probe (Dew Master, Edgetech Instrument, remote D-probe SC) and capacitive sensors (Almemo, FHAD 46C41A) in the range of

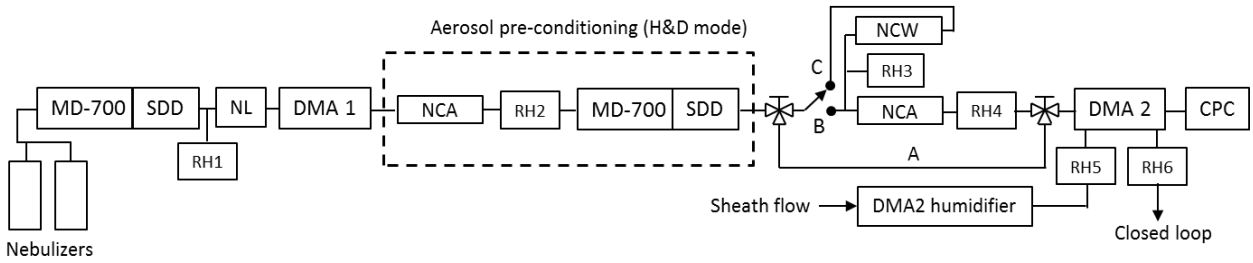

Fig. S2. Experimental setup of the high humidity tandem differential mobility analyzer (HHTDMA) system: MD-700 – NAFION dryer, SDD – silica gel diffusion dryer, RH – relative humidity sensor, NL – 85Kr aerosol neutralizer, DMA – differential mobility analyzer, NCA – Nafion conditioner with air, NCW – Nafion conditioner with water, CPC – condensation particle counter, Operation mode: A– hydration&dehydration (H&D), B – hydration, C – dehydration.

2-80 % RH and the ammonium sulfate scans at RH above 80 %. Based on the Extended Aerosol Inorganics Model (E-AIM, model II) (Clegg et al., 1998; Wexler and Clegg, 2002), we converted the measured ammonium sulfate growth factors into RH($g_{b,E-AIM}$). The residence time between the aerosol preconditioning system and DMA2 depends on the humidification mode; its minimum value is 6.5 s, which corresponds to RT in the hydration operation mode (Fig.S2). The algorithm used for calculating the uncertainty of RH and growth factors discussed in detail elsewhere (Mikhailov and Vlasenko, 2020). Figure S3 illustrates these uncertainties for the case of subpollen particles.

Table S2. Sequence of relative humidity ("RH history") experienced by the investigated aerosol particles in the key elements of the HHTDMA system (DMA1, conditioner, DMA2) during different types of HHTDMA experiments (modes of operation). For each type of experiment, *X* represents the independent variable, i.e., the RH value taken for plotting and further analysis of the measurement results.

HHTDMA experiment (operation mode)	DMA2 (size selection)	Conditioner (humidification)			DMA2 (size measurement)	
	RH1 (%)	RH2 (%)	RH3 (%)	RH4 (%)	RH5 (%)	RH6 (%)
Hydration and dehydration (H&D)	< 2	*X*	NU[a]	NU	< 2	< 2
Hydration	< 2	$RH_{H\&D.min}$[b]	NU	*X*	*X*	*X*
Dehydration	<2	$RH_{H\&D.min}$	> 96	*X*	*X*	*X*

[a] NU – not used

[b] $RH_{H\&D,.min}$ is the relative humidity that corresponds to the $D_{b.H\&,Dmin}$ obtained in H&D experiment.

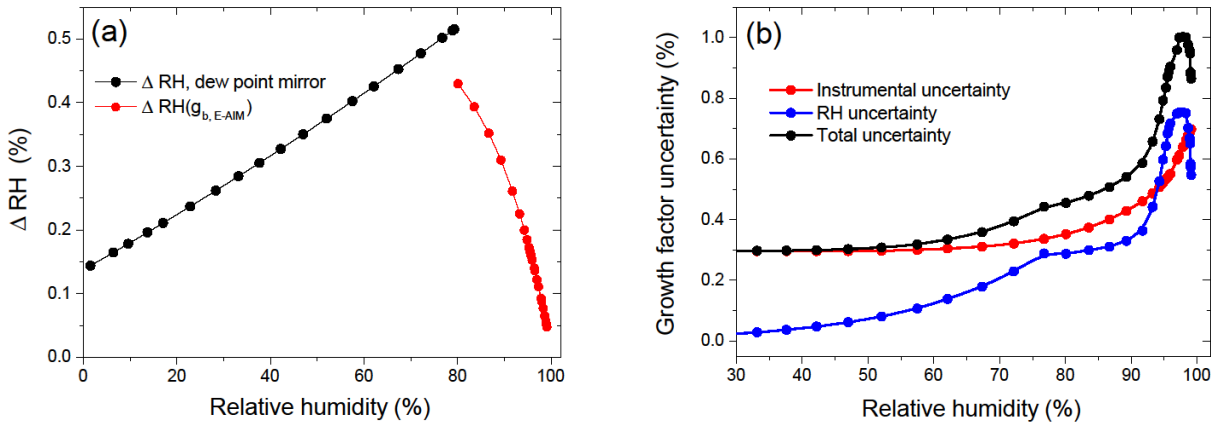

Fig. S3. Accuracy in RH using different methods (**a**) and relative growth factor uncertainty due to instrumental and RH errors.

S4. Conversion of DLS–based hydrodynamic size distribution into particle number size distribution

The size distribution obtained by DLS is based on the scattering intensity of the particles. For the case of Rayleigh particles, the scattering intensity is proportional to the sixth power of the diameter.

Thus, in term of intensity of light scattering the relative contribution, $f_{i,scat.}$ from each particle size bin is (Finsy, 1994; Li et al., 2014)

$$f_{i,scat.} = \frac{N_i D_i^6}{\sum N_i D_i^6} \quad , \tag{S1}$$

where N_i is the number of particles in size bin i having the mid-point diameter D_i. To convert the intensity-based size distribution into number particles size distribution ($f_{i,N}$) we let

$$x_i = \frac{f_{i,scat}}{D_i^6} \quad . \tag{S2}$$

As an example Fig. S4 shows the result of converting intensity-based size distribution of birch pollen colloids to a number-weighted distribution. Combining Eq. (S1) and Eq. (S2), we obtain normalized number particles size distribution:

$$f_{i,N} = \frac{x_i}{\sum x_i} \quad . \tag{S3}$$

If the suspended particles all have density ρ then their mass M_0 with respect to the total number N_0, is

$$M_0 = N_0 \rho \frac{\pi}{6} \sum_i f_{i,N} D_i^3 \quad . \tag{S4}$$

Total mass of suspended species in the filtered solution (M_0) was determined as the difference between the total mass of the solids in the filtered solution and the mass of dissolved species (Table 1), therefore N_0 can be calculated from Eq. (S4). If N_0 and $f_{i,N}$ are known the number of colloids in each size bin is $N_i = f_{i,N} N_0$. A material density of 1.4 g cm^{-3} was used for suspended organic particles suggesting that starch (1.53 g cm^{-3}), membrane proteins (1.37 g cm^{-3}), cellulose (1.5 g cm^{-3}), carotenoids (~1 g cm^{-3}) and lipids (1.0 -1.2 g cm^{-3}) (Haynes, 2011) are the main species in the series of water-insoluble pollen compounds (Stanley and Linskens, 1974).

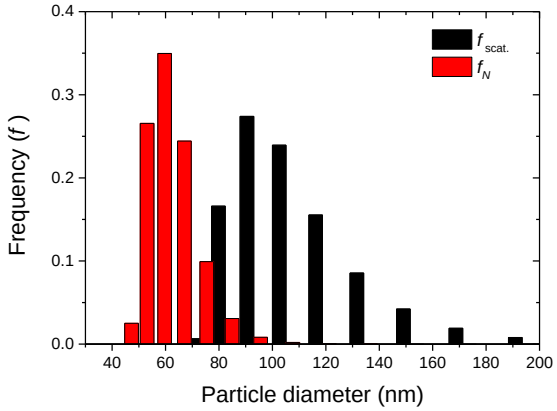

Fig. S4 Conversion of intensity-based size distribution ($f_{scat.}$) of birch pollen colloids to a number-weighted distribution (f_N).

It should be noted that the DLS-based size distributions in some cases has a high degree of uncertainty. In the DLS setup, the light scattered by fluctuations of the concentration of molecules, particles, or aggregates suspended in a tested solution is recorded. To determine the rates of decay of the intensity of the scattered light, the time correlation function, $g(\tau)$ of this intensity is analyzed. Since the correlation function is a superposition of exponential decays with distributed decay rates, the distribution function is the inverse Laplace transform of the correlation function. The CONTIN algorithm (Provencher, 1982; Scotti et al., 2015) carries out this transformation numerically. One of the limitations of the resolution comes from the extremely ill-conditioned nature of this Laplace inversion. Practically very small differences in $g(\tau)$ within typical experimental accuracy may result in quite different particle size distributions after inversion (Finsy, 1994; Anderson et al., 2013; Varenne et al., 2016). Both DLS data uncertainty and inversion algorithm together with approximations used in Eq. (S4) will provide an error in size distribution.

S5. Calculation of the κ uncertainty

Hygroscopicity parameter κ can be determined from an approximate formula (Petters and Kreidenweis, 2007):

$$\kappa_{app} = \frac{4A^3}{27D_a^3 ln^2 s_c} \quad with \quad A = \frac{4\sigma M_w}{\rho_w RT} \ . \tag{S5}$$

For the studied samples the difference between κ_a and κ_{app} calculated from Eq.(6) and its simplified form (Eq.S5) for $\kappa > 0.07$ on average did not exceed 2%. Therefore, CCNC-based κ_a uncertainty was calculated as Gaussian propagated error based on Eq. (S5) using experimental uncertainties associated with s_c and D_a:

$$\Delta\kappa_a = \sqrt{\left(-\frac{12A^3}{27D_a^4 ln^2 s_c}\Delta D_a\right)^2 + \left(-\frac{8A^3}{27 s_a D_a^3 ln^3 s_c}\Delta s_a\right)^2} \tag{S6}$$

Similarly, the HHTDMA-derived κ_b was obtained based on Eq.(7):

$$\Delta\kappa_b = \sqrt{\left(\frac{1-a_w}{a_w} 3g_b^2 \Delta g_b\right)^2 + \left(-\frac{g_b^3 - 1}{a_w^2}\Delta a_w\right)^2} \quad , \tag{S7}$$

where $\Delta a_w = (\Delta RH/RH) \cdot a_w$. Uncertainty in RH and g_b are shown in Fig. S3.

S6. Coagulation of hydrosols

Figure S5 shows a time-dependent light scattering of colloids in the birch pollen aqueous extract. The obtained results indicate that during the first 10 hours, the Tyndall effect caused by colloid

particles coagulation is negligible. However, it became essential after 10 hours. In the time scale of 20-50 h, the intensity of Reyleigh scattering (symmetrical phase function) progressively increasing. After 50 hours, large particles are formed with a loss of aggregate stability and the forward lobe of Mie scattering is dominant.

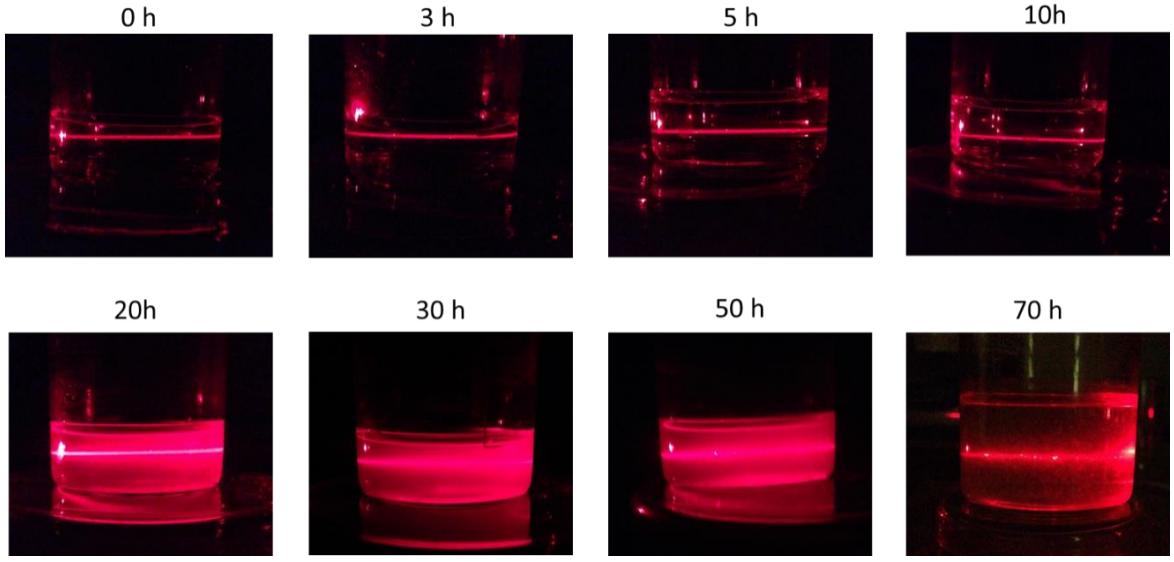

Fig. S5. A time-dependent light scattering of colloids in the birch pollen aqueous extract. The SPP concentration in the filtered solution was the same as used for HHTDMA and CCN measurements (Sect.2.1).

S7. Size dependent SPP restructuring

The obtained in hydration and dehydration (H&D) HHTDMA experiments minimum mobility growth factors, $g_{b,H\&D,min} = D_{b,RH}/D_{b.i}$ as a function of initial mobility diameter ($D_{b.i}$) (Fig. 4) were fitted by exponential curve (Eq.10). The best fit parameters are given in Table S3.

Table S3. The best fit parameters of Eq. (14). R^2 is the coefficient determination of the fit.

Species	η	φ	τ	R^2
Birch SPP	0.852	0.179	149.3	0.998
Pine SPP	0.861	0.178	117.0	0.996
Rapeseed SPP	0.905	0.145	72.30	0.998

S8. Envelope shape of rapeseed SPP.

The irregular shape morphology of the rapeseed SPP (Fig. 5c) approximated by a Ferret ellipsoid with maximal (a) and minimal (b) axis, respectively. The envelope shape factor, β calculated by assuming that in both DMA the particles are oriented to its flow by maximal axis (prolate ellipsoid) (Fuchs, 1964):

$$\beta = \frac{\frac{4}{3}(\alpha^2 - 1)}{\frac{2\alpha^2 - 1}{\sqrt{\alpha^2 - 1}} ln\left(\alpha + \sqrt{\alpha^2 - 1}\right) - \alpha}, \quad \text{(S8)}$$

where $\alpha = a/b$ is the aspect ratio. The calculated values of β are listed in Table S4.

Table S4. Envelope shape parameter (β) of rapeseed SPP as a function of size (b) and ellipsoid aspect ratio (α) estimated from SEM images using *ImageJ* processing software. Twenty images of each size range were used to calculate the average ± standard deviation aspect ratio.

b (nm)	a/b	β
60 ± 3	1.13 ± 0.11	1.03 ± 0.02
80 ± 4	1.16 ± 0.08	1.03 ± 0.02
100 ± 5	1.20 ± 0.11	1.04 ± 0.03
140 ± 7	1.32 ± 0.12	1.07 ± 0.03
180 ± 10	1.44 ± 0.10	1.09 ± 0.02

References

Anderson, W., Kozak, D., Coleman, V. A., Jämting, Å. K. and Trau, M.: A comparative study of submicron particle sizing platforms: Accuracy, precision and resolution analysis of polydisperse particle size distributions, J. Colloid Interf. Sci., 405, 322-330, https://doi.org/10.1016/j.jcis.2013.02.030, 2013.

Chichiriccò, G., Pacini, E., and Lanza, B.: Pollenkitt of some monocotyledons: lipid composition and implications for pollen germination, Plant. Biol., 21, 920-926, https://doi.org/10.1111/plb.12998, 2019.

Clegg, S. L., Brimblecombe, P., and Wexler, A. S.: A thermodynamic model of the system $H^+ – NH_4^+ – Na^+ – SO_4^{2-} – NO_3^- – Cl^- – H_2O$ at 298.15 K, J. Phys. Chem. A, 102, 2155–2171, https://doi.org/10.1021/jp973043j, 1998.

Finsy, R.: Particle sizing by quasi-elastic light scattering, Adv. Coll. Inter. Sci., 52, 79-143, https://doi.org/10.1016/0001-8686(94)80041-3, 1994.

Haynes, W. M. (ed.), CRC Handbook of Chemistry and Physics (92nd ed.). CRC Press. p. 394, 2011.

Li, Z., Wang, Y., Shen, J., Liu, W., and Sun, X.: The measurement system of nanoparticle size distribution from dynamic light scattering data, Opt. Laser Eng., 56, 94-98, http://dx.doi.org/10.1016/j.optlaseng.2013.12.004, 2014.

Mikhailov, E. F. and Vlasenko, S. S.: High-humidity tandem differential mobility analyzer for accurate determination of aerosol hygroscopic growth, microstructure, and activity coefficients over a wide range of relative humidity, Atmos. Meas. Tech., 13, 2035–2056, https://doi.org/10.5194/amt-13-2035-2020, 2020.

Pacini, E., and Franchi, G. G.: Role of the tapetum in pollen and spore dispersal. In: Hesse M., Pacini E., Willemse M. (eds). The Tapetum. Pl. Syst. and Evol. 7, 1-11, https://doi.org/10.1007/978-3-7091-6661-1_1, 1993.

Pacini, E. and Hesse, M.: Pollenkitt – its composition, forms and functions, Flora, 200, 399-415, https://doi.org/10.1016/j.flora.2005.02.006, 2005.

Petters, M. D. and Kreidenweis, S. M.: A single parameter representation of hygroscopic growth and cloud condensation nucleus activity, Atmos. Chem. Phys., 7, 1961–1971, https://doi.org/10.5194/acp-7-1961-2007, 2007.

Piffanelli, P., Ross, J. H. E., and Murphy, D. J.: Biogenesis and function of the lipidic structures of pollen grains, Sex. Plant Reprod., 11, 65–80, https://doi.org/10.1007/s004970050122, 1998.

Provencher, S. W.: A constrained regularization method for inverting data represented by linear algebraic or integral equations: Commun. Comput. Phys., 27, 213–227, https://doi.org/10.1016/0010-4655(82)90173-4, 1982.

Scotti, A., Liu, W., Hyatt, J. S., Hermann E. S., Chol, Y. S., Kim, J. W., Lyon. L. A., Gasser, U., and Fernandes-Nieves, A.: The CONTIN algorithm and its application to determine the size distribution of microgel suspensions, J. Chem. Phys., 142. 234905, https://doi.org/10.1063/1.4921686, 2015.

Stanley, R.G., and Linskens, H.F.: Pollen: Biology, Biochemistry and Management, Springer, Berlin, Heidelberg, 307 p., 1974.

Varenne, F., Makky, A., Gaucher-Delmas, M., Violleau, F., and Vauthier, C.: Multimodal dispersion of nanoparticles: A comprehensive evaluation of size distribution with 9 size measurement methods, Pharm. Res., 33, 1220-1234, https://doi.org/10.1007/s11095-016-1867-7, 2016.

Wexler, A. S. and Clegg, S. L.: Atmospheric Aerosol Models for Systems Including the Ions H^+, NH_4^+ , Na^+, SO_4^{2-} ,NO_3^- , Cl^-, Br^-, and H_2O, J. Geophys. Res., 107, 4207, https://doi.org/10.1029/2001JD000451, 2002.